Pet. Sci. (2015) 12:391–405
DOI 10.1007/s12182-015-0045-6

ORIGINAL PAPER

Factors influencing physical property evolution in sandstone mechanical compaction: the evidence from diagenetic simulation experiments

Ke-Lai Xi[1,3] · Ying-Chang Cao[1] · Yan-Zhong Wang[1] · Qing-Qing Zhang[1] · Jie-Hua Jin[1] · Ru-Kai Zhu[2] · Shao-Min Zhang[1] · Jian Wang[1] · Tian Yang[1] · Liang-Hui Du[1]

Received: 31 July 2014 / Published online: 28 July 2015

Abstract In order to analyze the factors influencing sandstone mechanical compaction and its physical property evolution during compaction processes, simulation experiments on sandstone mechanical compaction were carried out with a self-designed diagenetic simulation system. The experimental materials were modern sediments from different sources, and the experiments were conducted under high temperature and high pressure. Results of the experiments show a binary function relation between primary porosity and mean size as well as sorting. With increasing overburden pressure during mechanical compaction, the evolution of porosity and permeability can be divided into rapid compaction at an early stage and slow compaction at a late stage, and the dividing pressure value of the two stages is about 12 MPa and the corresponding depth is about 600 m. In the slow compaction stage, there is a good exponential relationship between porosity and overburden pressure, while a good power function relationship exists between permeability and overburden pressure. There is also a good exponential relationship between porosity and permeability. The influence of particle size on sandstone mechanical compaction is mainly reflected in the slow compaction stage, and the influence of sorting is mainly reflected in the rapid compaction stage. Abnormally high pressure effectively inhibits sandstone mechanical compaction, and its control on sandstone mechanical compaction is stronger than that of particle size and sorting. The influence of burial time on sandstone mechanical compaction is mainly in the slow compaction stage, and the porosity reduction caused by compaction is mainly controlled by average particle size.

Keywords Primary porosity · Mechanical compaction · Unconsolidated sand · Diagenetic simulation experiment

✉ Ke-Lai Xi
kelai06016202@163.com

✉ Ying-Chang Cao
cyc8391680@163.com

[1] School of Geosciences, China University of Petroleum, Qingdao, Shandong 266580, China

[2] Research Institute of Petroleum Exploration and Development, CNPC, Beijing 100083, China

[3] Department of Geosciences, University of Oslo, Oslo 0316, Norway

Edited by Jie Hao

1 Introduction

With increasing oil and gas exploration and the growing demand for oil and gas reserves, the oil and gas exploration targets of clastic rocks have turned to low porosity and permeability reservoirs, even to tight sandstone reservoirs, and they have gradually become the main source of increasing reserves and production of oil and gas (Wang and Tian 2003; Dai et al. 2012; Hart 2006; Zou et al. 2013; Tobin et al. 2010; Jia et al. 2012; Worden et al. 2000; Bloch et al. 2002; Wang et al. 2010; Zhang et al. 2011). Mechanical compaction, as one of the major destructive aspects of diagenesis, can cause dramatic changes in sandstone pore structure and distribution. It results in a substantial reduction of pore space, which is the main factor that damages reservoirs and forms low porosity, low permeability reservoirs (Zhu et al. 2008; Chester et al. 2004; Zhu et al. 2013; Lv and Liu 2009; Maast et al. 2011; Taylor et al. 2010; Ajdukiewicz et al. 2010; Zhang et al. 2008; Wang et al. 2015; Zhang et al. 2014; Liu et al. 2014). Previous studies have suggested that mechanical

compaction is influenced by a combination of various factors such as burial depth, sediment composition, particle size, sorting, abnormally high pressure, and burial time (Liu et al. 2007; Aplin et al. 2006).

However, current studies about various factors influencing compaction mainly focus on simple and qualitative description, and little work has been done on quantitative analysis based on simulation experiments, leading to the vague understanding of the evolution of physical properties and influencing mechanisms of various factors during mechanical compaction processes. This directly restricts the accurate characterization of the formation of low porosity and permeability sandstone reservoirs and their densification processes. Therefore, carrying out sandstone mechanical compaction simulation experiments and understanding the evolution of physical properties and the influencing mechanisms of various factors during mechanical compaction have not only an important theoretical significance for diagenesis, but also an important practical significance in physical property prediction of low porosity and permeability reservoirs.

2 Experimental facility and experimental procedures

The experiment was carried out in the Diagenetic Simulation Laboratory of China University of Petroleum, using a self-designed diagenetic simulation experiment system. This facility consists of two modules: the porosity and permeability testing module and the diagenetic simulation module. It measures sandstone porosity and permeability, simulating the high temperature and pressure conditions of subsurface strata, and monitoring physical property changes of sandstones in the course of diagenesis in real time. The sandstone mechanical compaction simulator is mainly composed of a constant current–constant voltage (CCCV) pump, intermediate container group, displacement sensors, axial compression control pump, core holder (with a built-in heating device), back-pressure booster pump, fluid-receiving scale, and automatic control system (Fig. 1). The upper temperature limit of the system is 300 °C, and the pressure limit is 80 MPa.

During sandstone mechanical compaction simulation experiments, the sample is in the core holder with movable pistons covering both ends. The axial compression pump is used to simulate overburden pressure and the micro back-pressure booster pump is manually operated to control the fluid pressure. A built-in core holder heating device and temperature control system are used to simulate the strata temperature. Precision displacement sensors at both ends of the core holder (with an accuracy of 0.001 mm) record compaction displacements. The intermediate container group is used to contain the fluid required for the experiment. The CCCV pump provides the displacement pressure to displace fluid and pore water toward the fluid-receiving scale at a constant flow rate. The automatic control system is used for measuring and recording sandstone permeability in real time.

3 Experimental design

3.1 Experimental samples

3.1.1 Sample collection

The samples selected for experiments were modern unconsolidated sands ranging from 5 to 20 cm below from the surface at Golden Beach and Silver Beach, Qingdao; Yellow River Estuary, Dongying; point bar, Mazhan River, Weifang; and mouth bar, Feng River, Jiaonan eastern China. During the sampling process, in order to keep the original packing state (grain combination sequence, sorting, etc.), we used copper tubes with a length of 140 mm and an inner diameter of 25.7 mm to take samples (Fig. 2). Two samples were collected within a distance of about 15 mm in each group, of which one was used for sandstone

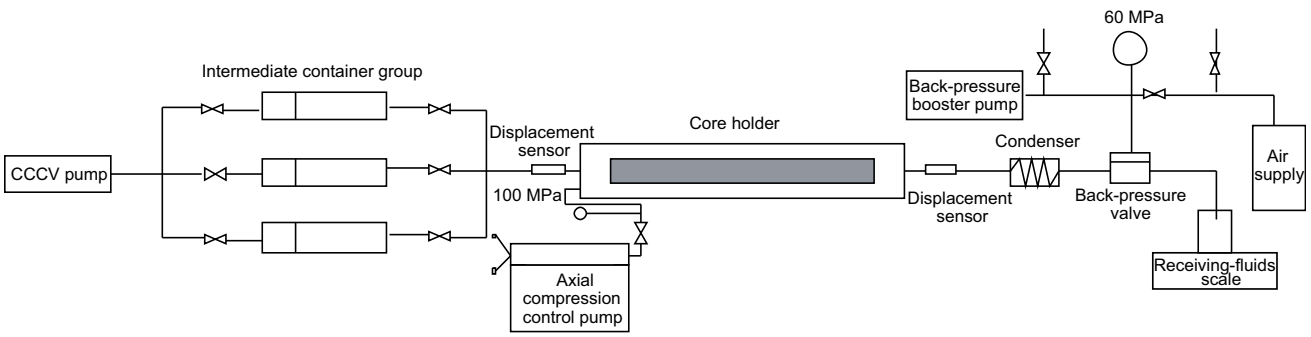

Fig. 1 Sandstone mechanical compaction simulation diagram

Fig. 2 Collection of experimental samples

Table 1 The parameters of experimental samples with different sources

Sample sources	Sample no.	Median particle size (*Md*), mm	Average particle size (*M*), mm	Sorting coefficient (*So*)	Initial length of samples (L_0), mm	Primary porosity (φ_0), %	Primary permeability (K_0), $\times 10^{-3}\mu m^2$
Silver Beach of Qingdao	I	0.215	0.219	1.556	88.5	42.96	696.7
Silver Beach of Qingdao	II	0.260	0.262	1.575	88.8	42.92	1779.9
Golden Beach of Qingdao	III	0.280	0.293	1.860	84.7	37.37	570.56
Yellow River Estuary of Dongying	IV	0.076	0.079	1.618	88.5	43.72	372.9
Mazhan River of Weifang	V	1.25	1.28	3.571	90.5	33.62	733.34
Silver Beach of Qingdao	VI	0.217	0.221	1.50	87.6	41.75	445.15
Yellow River Estuary of Dongying	VII	0.076	0.078	1.622	88.7	43.72	389.54
Feng River Estuary of Jiaonan	VIII	0.952	0.964	2.52	86.9	35.87	437.7

mechanical compaction simulation experiments and the other was for granularity parameter analysis. It was assumed that granularity parameters of the two samples were the same.

3.1.2 Laboratory analysis of samples

Firstly, the sand samples selected for simulation experiments were processed to 90 mm long with both ends flat, and they were covered by metal filters to prevent sands from becoming loose and sliding. Then the sand samples of each group were dried using a 101-1A-type electrothermal drying box. Finally, after being dried completely, one sand sample of each group for the mechanical compaction simulation experiment was put into the core holder, and then the primary porosity and permeability were measured using the porosity and permeability testing module (Table 1). Meanwhile, the corresponding other sand sample was used for granularity parameter analysis using sieve analysis method to obtain parameters such as median particle size (*Md*), average particle size (*M*), and sorting coefficient (*So*) (Table 1).

The sediments from Golden Beach and Silver Beach, Qingdao are mainly feldspar and quartz, with a relatively low content of volcanic rock debris and little biotite and magnetite, and the content of feldspar is higher than that of quartz. The content of rigid particles, e.g., feldspar and quartz, ranges from 70 % to 80 %, while the content of ductile particles like eruptive rock and mica is generally less than 20 %. The content of quartz is relatively higher than that of feldspar in the sediments from the Mazhan and Feng Rivers, with a low content of volcanic rock debris and visible chert. The content of rigid particles is over 85 % and that of ductile particles is less than 15 %. Sediments from Yellow River Estuary, Dongying are fine grained, with a low content of rigid particles and a high clay mineral content, which results in strong ductility.

3.2 Experimental conditions

To simulate the geological conditions of the Dongying Sag of the Jiyang Depression, Bohai Bay Basin in eastern China, the experimental conditions were set as follows: the geothermal gradient is 3.5 °C/100 m (average paleogeotherm gradient), the average formation density is about 2.4 g/cm^3, the average surface temperature is 18 °C, and the pressure coefficient under normal compaction is 1.0 (Liu et al. 2006). In order to simulate a pure mechanical compaction, distilled water was used as the fluid medium. Previous studies have shown that overpressure can develop

Table 2 Reference list of temperature and pressure experimental conditions

Simulated burial depth, m	Overburden pressure, MPa			Framework pressure, MPa	Fluid pressure, MPa			Temperature, °C
	Pressure coefficient 1.0	Pressure coefficient 1.2	Pressure coefficient 1.4		Pressure coefficient 1.0	Pressure coefficient 1.2	Pressure coefficient 1.4	
0	0	0	0	0	0	0	0	18
100	2.18	2.18	2.18	1.2	0.98	0.98	0.98	21.5
200	4.36	4.36	4.36	2.4	1.96	1.96	1.96	25
400	8.72	8.72	8.72	4.8	3.92	3.92	3.92	32
600	13.08	13.08	13.08	7.2	5.88	5.88	5.88	39
800	17.44	17.44	17.44	9.6	7.84	7.84	7.84	46
1000	21.8	21.8	21.8	12	9.8	9.8	9.8	53
1200	26.16	26.16	26.16	14.4	11.76	11.76	11.76	60
1400	30.52	30.52	30.52	16.8	13.72	13.72	13.72	67
1600	34.88	38.016	41.152	19.2	15.68	18.816	21.952	74
1800	39.24	42.768	46.296	21.6	17.64	21.168	24.696	81
2000	43.6	47.52	51.44	24	19.6	23.52	27.44	88
2200	47.96	52.272	56.584	26.4	21.56	25.872	30.184	95
2400	52.32	57.024	61.728	28.8	23.52	28.224	32.928	102
2600	56.68	61.776	66.872	31.2	25.48	30.576	35.672	109
2800	61.04	66.528	72.016	33.6	27.44	32.928	38.416	116
3000	65.4	71.28	77.16	36	29.4	35.28	41.16	123

below 1600 m in the Dongying Sag (Liu et al. 2009). According to the stress–burial depth conversion formula 0.02262 MPa = 1 m (Gluyas and Cade 1999), the strata pressure at 1600 m is approximately 36.16 MPa. Therefore, taking the above geological factors into account, as well as the applicable temperature and pressure conditions of the facility, we designed a temperature and pressure reference list for sandstone mechanical compaction under normal compaction conditions with a pressure coefficient of 1.0 and under overpressure conditions with pressure coefficients of 1.2 and 1.4 for contrast experiments. In this way, the evolution of physical properties and the influencing factors during the simulation process of sandstone mechanical compaction can be analyzed (Table 2).

3.3 The calculation of porosity and permeability

3.3.1 Porosity calculation

The porosity calculation method during the simulation process of sandstone mechanical compaction is as follows:

$$S_0 = \pi r^2; \tag{1}$$

$$V_0 = L_0 S_0; \tag{2}$$

$$V_\Phi = V_0 - V_g; \tag{3}$$

$$\Phi_0 = V_\Phi / V_0 \times 100\ \%. \tag{4}$$

Here, r is the cross-sectional radius of sample, cm, L_0 is the initial length of sample, cm, S_0 is the cross-sectional area of sample, cm^2, V_0 is the initial volume of sample, cm^3, V_Φ is the initial pore volume of sample, cm^3, V_g is the framework volume of sample, cm^3, and Φ_0 is the primary porosity, %.

Primary porosity Φ_0 could be measured by the porosity and permeability testing module of the diagenetic simulation system (Table 1).

Therefore, sample volume at each pressure point during compaction could be calculated with the recorded compaction displacement:

$$V = S_0(L_0 - L_1). \tag{5}$$

Here, L_1 is the recorded compaction displacement, cm, V is the sample volume at each pressure point during compaction, cm^3.

The loss of sample volume during compaction mainly consists of intergranular pore volume during the experiment by assuming the framework volume as a constant, thus:

$$V_0 - V_\Phi = V - V \times \Phi, \tag{6}$$

$$\Phi = (V - V_0 + V_\Phi)/V \times 100\%. \tag{7}$$

3.3.2 Permeability calculation

Permeability during the simulation of sandstone mechanical compaction can be calculated using Darcy's law.

$$K = Q\mu L/(\Delta P S_0). \quad (8)$$

That is

$$K = Q\mu(L_0 - L_1)/(\Delta P S_0). \quad (9)$$

Here, Q is the quantity of flow through the sample per unit time, cm^3/s, S_0 is the cross-sectional area of the sample, cm^2, μ is the fluid viscosity, $\times 10^{-3}$Pa s, L_0 is the original length of the sample, cm, L_1 is the recorded compaction displacement, cm, and ΔP is the pressure differential before and after fluid flowing through the sample, MPa.

The above K in Eq. (9) is the sample's permeability. It shows fluid flow capacity through the sample within a certain pressure differential.

Primary permeability K_0, permeability without compaction, could be measured by the porosity and permeability testing module after constant fluid passing through (Table 1). During the experiment, the fluid viscosity was set as 1×10^{-3} Pa s and other parameters were recorded by the automatic control system in real time, and then permeability variations could be calculated.

There is a close relationship between fluid viscosity (μ) and temperature (T). Therefore, on the basis of reviewing water viscosities at different temperatures (Yuan 1985), an empirical formula can be fitted as follows:

$$T = 1.056233e^{-0.018118\mu} \quad R^2 = 0.976362. \quad (10)$$

We calculated fluid viscosity at different temperatures using Eq. (10) and then corrected the recorded permeability values.

3.4 Data acquisition and processing

Detailed procedures of data acquisition and processing during sandstone mechanical compaction simulation experiment are as follows:

First, according to the reference list of temperature and pressure conditions, we set the experimental temperature and pressure and then conducted mechanical compaction simulation experiments. After compaction at each pressure point was stable (the compaction displacement was a constant), we recorded the data with a fixed time interval of 2 min, and the record time of each pressure point was about 120 min, that is, there were 60 sets of record data. The recorded experimental parameters included experimental time, overburden pressure, fluid pressure, fluid flow, pressure differential between the ends of the core, experimental temperature, compaction displacement, and permeability. In the normal compaction simulation experiments, the upstream pressure on the sample is higher than the downstream pressure, so the fluid can be discharged onto the fluid-receiving scale in time. In the undercompaction simulation experiments, the differential between upstream pressure and downstream pressure was respectively set according to the pressure coefficients of 1.2 and 1.4, making the downstream pressure higher than the upstream pressure. In this way, fluid discharge was blocked and abnormally high pressure was formed.

Second, according to the compaction displacement, we calculated the corresponding porosity value of each data point.

Third, according to the relationship between viscosity and temperature, we corrected the corresponding permeability value of each data point.

Fourth, we precisely analyzed the data of overburden pressure, fluid pressure, temperature, porosity and permeability, and excluded abnormal data points caused by system errors.

Fifth, we calculated the average value of each parameter including overburden pressure, fluid pressure, temperature, porosity, and permeability after removing the abnormal data points, and regarded the average value as the experimental result of each pressure point to conduct experimental analysis and discussion.

4 Experimental results

According to experimental purposes, normal compaction simulation experiments were conducted on samples I, II, III, IV, and V, while with the simulated burial depth below 1600 m (overburden pressure was approaching 36.16 MPa), undercompaction simulation experiments with pressure coefficients of 1.2 and 1.4 were conducted on samples VI and VII, respectively. After data acquisition and processing of each sample, the experimental results can be obtained as follows (Tables 3, 4).

5 Discussion

5.1 Sandstone primary porosity analysis

Primary porosity is defined as the porosity of newly formed sediment. It is the starting point of porosity evolution during the reservoir burial process, and directly influences the accuracy of study of porosity evolution and is of great significance to reservoir porosity prediction.

Table 3 Experimental results of several samples under normal compaction

Sample I				Sample II				Sample III			
Overburden pressure, MPa	Fluid pressure, MPa	Porosity, %	Permeability, $\times 10^{-3}$ μm^2	Overburden pressure, MPa	Fluid pressure, MPa	Porosity, %	Permeability, $\times 10^{-3}$ μm^2	Overburden pressure, MPa	Fluid pressure, MPa	Porosity, %	Permeability, $\times 10^{-3}$ μm^2
0.00	0.00	42.96	696.7	0.00	0.00	42.92	1779.9	0.00	0.00	37.37	570.56
2.05	0.95	42.22	386.63	2.39	1.01	42.4	888.7	2.3	1.11	37.08	391.05
4.4	2.05	41.81	198.17	4.71	2.01	42.16	744.4	5.29	2.6	36.48	202.53
8.62	4.12	41.41	126.17	9.24	4.47	41.79	218.2	8.61	4.11	34.62	134.69
12.97	6.07	40.9	103.69	12.85	5.77	41.45	152.4	12.84	6.1	31.98	103.8
17.47	8.14	40.45	65.67	16.68	7.35	41.43	143.1	17.63	8.43	31.26	56.69
21.38	10	40.07	43.92	21.96	9.9	40.94	97.9	21.18	10.09	31.1	46.39
26.19	12.3	39.78	31.78	26.16	11.95	40.53	76.02	25.82	12.1	30.84	37.47
30.1	14.2	39.44	23.63	30.47	13.87	40.17	50.6	30.15	14.06	30.56	30.06
34.88	16.3	39.09	21.6	34.62	16.03	39.97	44.9	34.35	16.21	30.32	25.58
39.15	17.9	38.72	18.53	39.09	18.31	39.69	32.9	39.09	18.48	30	22.1
43.44	20	38.46	14.08	43.66	20.09	39.46	23.8	42.46	20.12	29.7	19.3
48.53	22.2	38.16	13.24	48.47	22.43	39.2	19.6	46.72	22.1	29.45	14.41
52.09	23.9	37.93	12.23	52.38	23.99	38.99	14.6	51.85	24.25	29.28	11.47
55.45	26.4	37.57	8.45	57	26.03	38.8	12.9	57.19	26.21	28.94	11.28
63.25	29.4	37.12	7.24	61.09	27.73	38.59	10.9	–	–	–	–
65.16	30	36.67	5.44	65.45	29.47	38.49	9.4	–	–	–	–

Sample IV				Sample V			
Overburden pressure, MPa	Fluid pressure, MPa	Porosity, %	Permeability, $\times 10^{-3}$ μm^2	Overburden pressure, MPa	Fluid pressure, MPa	Porosity, %	Permeability, $\times 10^{-3}$μm^2
0.00	0.00	43.72	372.9	0.00	0.00	33.62	733.72
1.99	0.95	43.09	286.02	2.31	0.95	33.51	353.34
4.25	2.13	42.82	240.53	4.5	2.13	32.66	230.81
8.56	4.05	42.37	151.02	8.88	4.15	31.24	125.35
12.63	6.04	42.03	111.01	13.24	5.97	30.3	112.54
17.83	8.64	41.66	74.2	17.54	7.91	29.58	24.4
21.38	9.91	41.45	64.15	21.84	9.8	28.89	17.82
25.76	12.09	41.19	53.7	26.1	11.91	28.08	15.79
30.39	13.93	40.82	40.33	30.78	13.91	27.36	13.06
34.88	16.02	40.54	36.41	35.2	15.91	26.74	11.34
39.29	18	40.23	33.2	39.21	17.97	26.35	9.82
43.4	19.95	39.99	20.63	43.23	19.9	25.82	8.33

Table 3 continued

Sample IV				Sample V			
Overburden pressure, MPa	Fluid pressure, MPa	Porosity, %	Permeability, $\times 10^{-3}$ μm^2	Overburden pressure, MPa	Fluid pressure, MPa	Porosity, %	Permeability, $\times 10^{-3}$ μm^2
46.74	22.19	39.73	17.44	48.4	21.78	25.38	6.95
52.59	23.99	39.45	15.85	52.88	24.02	24.95	6.43
56.29	26.14	39.26	13.01	56.92	25.95	24.5	4.92
63.41	29.69	39.02	10.56	61.6	28.32	24.24	4.28
70.32	31.85	38.61	6.74	66	29.79	23.93	3.49

Previous studies have shown that primary porosity is influenced by a combination of parameters such as particle size, sorting, and sphericity, of which particle size and sorting are the most important factors influencing primary porosity and particularly the influence of sorting is more pronounced (Beard and Weyl 1973; Folk and Ward 1957; Rogers and Head 1961). Therefore, the average particle size and sorting coefficient were analyzed for their influences on primary porosity. Results show that there is a logarithmic relationship between primary porosity and particle size as well as sorting (Fig. 3).

$$\Phi_0 = -3.652\ln(M) + 35.744 \quad R^2 = 0.7755, \tag{11}$$

$$\Phi_0 = -12.61\ln(So) + 48.508 \quad R^2 = 0.8621, \tag{12}$$

where M is average particle size, So is sorting coefficient, and Φ_0 is primary porosity.

The primary sandstone porosity is influenced by a combination of sorting coefficient and average particle size. Moreover, predicting or estimating the dependent variable using the optimal combination of multiple independent variables is more effective and realistic than using only one independent variable (Hu et al. 2013). Therefore, the binary function relationship among primary porosity and average particle size and sorting coefficient is established with a stepwise regression method.

$$\Phi_0 = -3.0413So - 3.4907M + 47.828123. \tag{13}$$

Stepwise regression results show that the multiple correlation coefficient is 0.9031177, the average deviation is small and the precision is high (Table 5).

5.2 Physical property evolution during sandstone mechanical compaction

According to the above experimental conditions and the relation of overburden pressure and depth (Gluyas and Cade 1999), the overburden pressure can be converted into approximate depth (Fig. 4). The analysis shows that the evolution of porosity and permeability has a segmentation characteristic with the increasing overburden pressure and depth during mechanical compaction, and the evolution trend line can be divided into two stages. During the earlier stage of mechanical compaction, when the overburden pressure is less than 12 MPa and the equivalent burial depth is shallower than 600 m, with pressure increasing, detrital particles slide, displace, and rotate to rearrange and adjust their positions so that they can achieve a close-packing state with minimum potential energy. At this stage, i.e., the rapid compaction stage, porosity and permeability decrease rapidly (Fig. 4). Afterwards, detrital particles reach a stable packing state. With increasing pressure, the degree of close packing increases, and

Table 4 Experimental results of several samples under overpressure conditions

Sample VII				Sample VI			
Overburden pressure, MPa	Fluid pressure, MPa	Porosity, %	Permeability, $\times 10^{-3}$ μm^2	Overburden pressure, MPa	Fluid pressure, MPa	Porosity, %	Permeability, $\times 10^{-3}$ μm^2
0	0	43.72	389.54	0	0	41.75	445.15
1.93	0.97	42.53	147.852	2.36	1.22	41.25	399.29
4.74	2.36	42.09	103.387	4.28	2.01	41.07	307.98
8.64	4.21	41.56	76.359	8.67	4.12	40.75	221.32
17.33	8.02	40.12	43.347	13.56	6.36	40.41	130.06
21.86	10.01	39.85	36.832	17.45	8.02	40.19	88
26.03	11.95	39.58	26.841	19.39	9.01	40.04	–
29.97	13.97	39.30	23.693	28.94	13.68	38.99	56.86
41.49	22.38	39.01	16.971	35.38	16.09	38.83	30.57
46.55	25.39	38.87	14.515	39.89	21.56	38.77	33.12
51.51	27.96	38.72	12.882	43.62	23.65	38.60	24.24
57.12	30.82	38.58	10.075	48.21	26.37	38.44	21.86
62.01	33.73	38.42	8.33	51.32	28.52	38.23	16.42
68.19	36.47	38.23	5.557	56.98	31.34	38.09	–
71.89	38.63	38.08	4.078	57.41	34.23	37.64	10.88
–	–	–	–	68.64	35.72	37.63	8.8

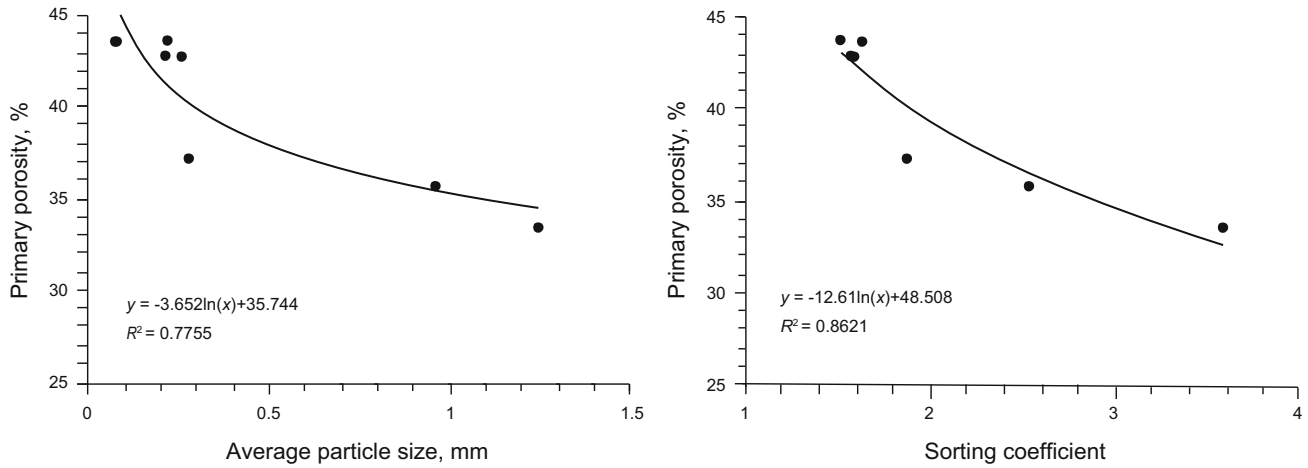

Fig. 3 Relationship between primary porosity and particle size as well as sorting coefficient

porosity and permeability decrease slowly. This is, the slow compaction stage (Fig. 4).

The experimental data from the slow compaction stage can be used to analyze the evolution of porosity and permeability with increasing overburden pressure during normal compaction (Liu et al. 2006). Regression analysis results show that there is an exponential relationship between porosity and overburden pressure, and the relationship can be expressed as $y = Ae^{Bx}$; while a power function relationship exists between permeability and overburden pressure, that is $y = Cx^D$. Meanwhile, the relationship between porosity and permeability is exponential (Table 6).

According to the comparison of experimental results of different samples, the coefficient A of the functional relationship $y = Ae^{Bx}$ between overburden pressure and porosity mainly depends on the primary porosity value, which is mainly controlled by the sorting coefficient. While the coefficient B is principally influenced by the average particle size. The coefficient C of the functional

Table 5 Stepwise regression results of sandstone primary porosity and average particle size and sorting coefficient

Sample no.	Sorting coefficient *So*	Average particle size *M*, mm	Regression value	Original value	Deviation
I	1.556	0.219	42.345378	42.959999	0.614621
II	1.575	0.262	41.193932	37.369999	−3.823933
III	1.860	0.293	42.130514	42.919998	0.789484
IV	1.618	0.079	42.642020	43.720001	1.077982
V	3.571	1.28	32.604338	33.619999	1.015661
VI	1.50	0.221	42.494747	41.750000	0.744747
VII	2.52	0.964	36.799067	35.869999	–0.929068

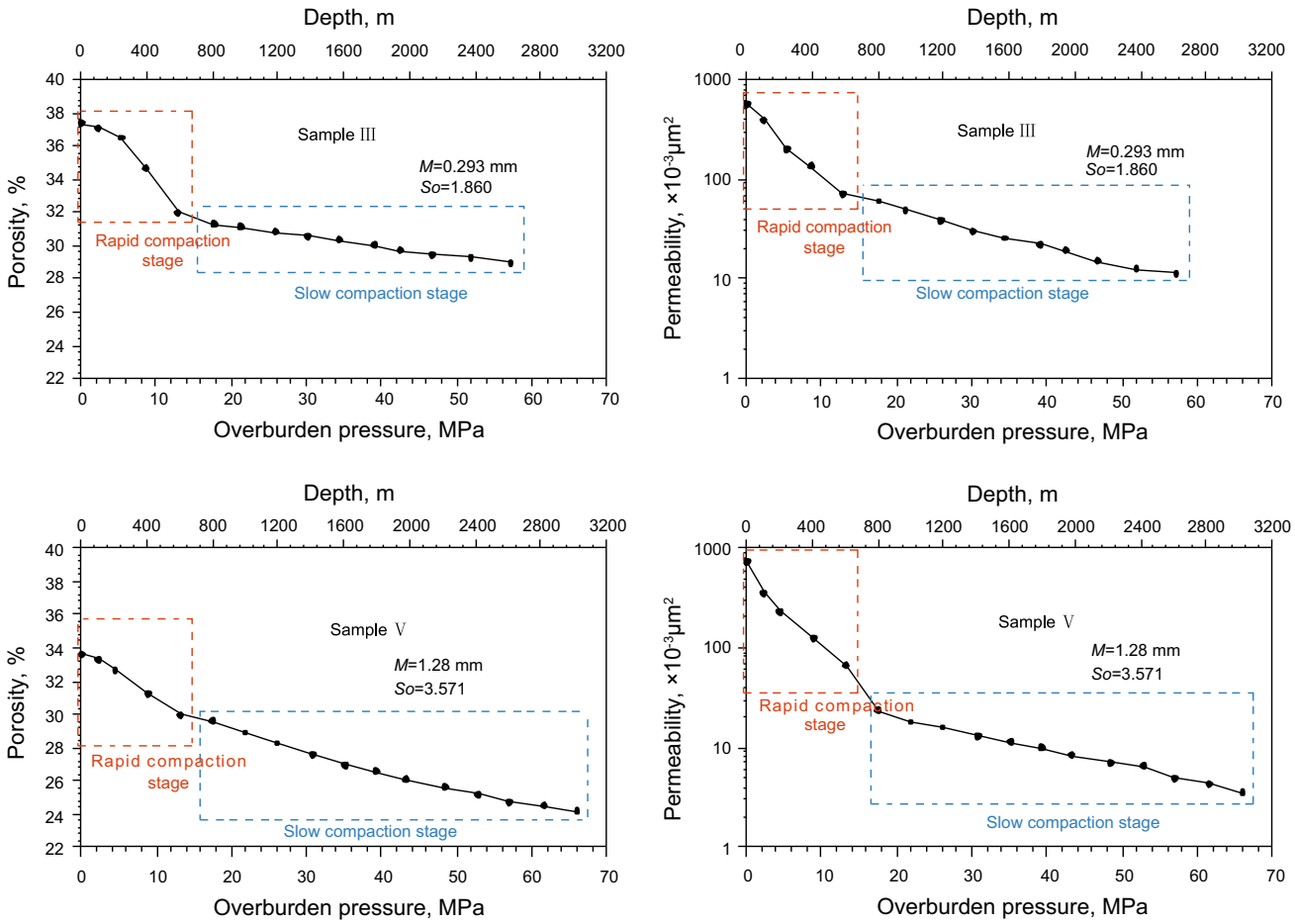

Fig. 4 Variation of porosity and permeability with increasing overburden pressure and depth during normal compaction

relationship $y = Cx^D$ is mainly controlled by the average particle size, while the coefficient D is greatly influenced by the sorting coefficient.

5.3 The influence of particle size on sandstone mechanical compaction

Sample I and sample II are characterized by the same composition, similar sorting, but different average particle sizes. Sample I is fine sand, but sample II is medium sand. Simulation experiment results show that two samples have approximately equal primary porosity (Table 1). During the rapid compaction stage, the evolution processes of two samples are almost the same. After entered into the slow compaction stage, the decrease rate of porosity of sample II with coarser average particle size is obviously smaller than that of sample I with finer average particle size during the increasing overburden pressure process. Meanwhile, the

Table 6 Evolution of porosity and permeability with overburden pressure under normal compaction

Sample no.	The relation between overburden pressure (x) and porosity (y)	The relation between overburden pressure (x) and permeability (y)	The relation between porosity (x) and permeability (y)
I	$y = 41.82372e^{-0.00193x}$ $R^2 = 0.99456$	$y = 8{,}761.51262x^{-1.70980}$ $R^2 = 0.97494$	$y = 8E - 10e^{0.6146x}$ $R^2 = 0.9796$
II	$y = 42.18101e^{-0.00148x}$ $R^2 = 0.98048$	$y = 61{,}210.68436x^{-2.08359}$ $R^2 = 0.98755$	$y = 1E - 15e^{0.9534x}$ $R^2 = 0.9939$
III	$y = 32.43762e^{-0.00201x}$ $R^2 = 0.99545$	$y = 3777.39155x^{-1.43168}$ $R^2 = 0.97816$	$y = 2E–08e^{0.6991x}$ $R^2 = 0.9816$
IV	$y = 42.72003e^{-0.00148x}$ $R^2 = 0.99416$	$y = 22{,}104.72226x^{-1.86625}$ $R^2 = 0.93290$	$y = 3E–13e^{0.7989x}$ $R^2 = 0.9827$
V	$y = 31.48912e^{-0.00436x}$ $R^2 = 0.98478$	$y = 2{,}491.68733x^{-1.53245}$ $R^2 = 0.97417$	$y = 0.00094e^{0.34938x}$ $R^2 = 0.97009$

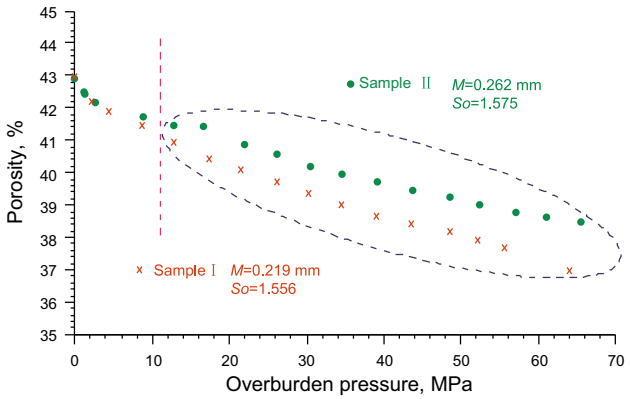

Fig. 5 Influence of particle size on sandstone mechanical compaction

difference of the remaining porosity of the two samples is more significant (Fig. 5).

By quantitative analysis of experimental data, the porosity reduction of sample I is 6.29 %, which is obviously larger than that of sample II 4.43 % when the overburden pressure increases to 65 MPa. Studies of different compaction stages show that during the rapid compaction stage, the average porosity reduction of sample I and sample II is 0.339 % and 0.334 %, respectively, with 2.3 MPa increase of the overburden pressure (about 100 m of the burial depth, the same below), which is almost the same. However, during the slow compaction stage, the porosity reduction of sample I is 0.197 %, which is larger than that of sample II 0.156 % with 2.3 MPa increase of the overburden pressure (Table 7).

Therefore, the influence of particle size on mechanical compaction is mainly in the slow compaction stage during the burial process of sandstone. The coarser the particle size, the slower the compaction rate and the larger the final porosity. The influence of the particle size on mechanical compaction is more pronounced with increasing burial depth and overburden pressure. After experienced the rapid compaction, detrital particles are generally in contact with each other. The sample with finer particle size has a larger specific surface area and thus a smaller force per unit area. Sliding deformation does not occur easily with increasing overburden pressure which is mainly used to squeeze the pore space, resulting in the rapid loss of porosity. While the sample with coarser particle size has a smaller specific surface area and thus a larger force per unit area, so sliding deformation occurs with increasing overburden pressure which offsets a portion of force squeezing the pore space, and the rate of porosity loss decreases.

Table 7 Data about the influence of particle size on sandstone mechanical compaction

Sample no.	I	II
Average particle size M, mm	0.219	0.262
Sorting coefficient So	1.556	1.575
Primary porosity Φ_0, %	42.96	42.92
Porosity loss with 65 MPa overburden pressure, %	6.29	4.43
Porosity loss during rapid compaction stage, %/2.3 MPa	0.339	0.334
Porosity loss during slow compaction stage, %/2.3 MPa	0.197	0.156

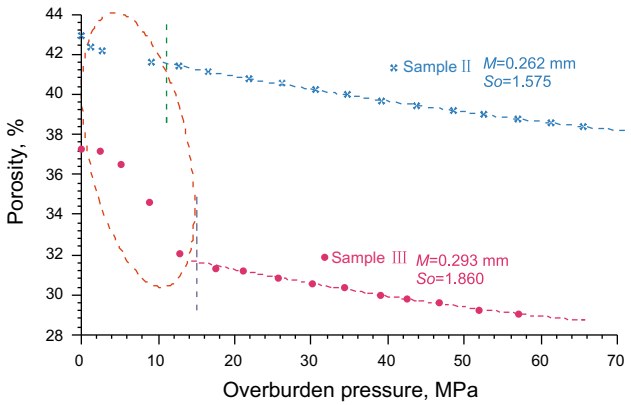

Fig. 6 Influence of sorting on sandstone mechanical compaction

5.4 The influence of sorting on sandstone mechanical compaction

Sample II and sample III selected from the Golden Beach and Silver Beach, Qingdao, eastern China are characterized by the same composition, similar particle size of medium sand, but different sorting, of which sample III has poorer sorting. Simulation experiment results show that sample III with poorer sorting has a smaller primary porosity (Table 1). During the rapid compaction stage, a great difference exists between the porosity evolution processes of the two samples, and the porosity reduction rate of sample III is significantly greater than that of sample II. After entered into the slow compaction stage, the evolution processes of the two samples are almost the same with increasing overburden pressure (Fig. 6).

The experimental results of different compaction stages show that during the rapid compaction stage, the average porosity loss of sample II is 0.334 % per 2.3 MPa increase of overburden pressure and the average porosity loss of sample III is 0.886 %, which is 2.65 times greater than that of sample II. However, the average porosity reduction of sample II and sample III is 0.156 % and 0.127 %, respectively, per 2.3 MPa increase of overburden pressure during the slow compaction stage, which is similar, and the porosity loss is in a negative relation to the average particle size (Table 8).

Therefore, the influence of sorting on sandstone mechanical compaction is mainly in the rapid compaction stage. The poorer the sorting, the higher the compaction rate and the more distinct the difference between the rapid compaction stage and the slow compaction stage. Also the dividing overburden pressure of the two stages will be larger (Fig. 6), that is, the rapid compaction stage lasts longer, and the equivalent burial depth is deeper. During the rapid compaction stage, for the sandstone sample with poorer sorting, when the position adjustment and rearrangement of detrital particles occur, finer particles will easily fill in the pore space formed by the arrangement of coarse particles, which results in a rapid loss of porosity. However, after entering the slow compaction stage, particles have a stable packing state, compaction further increases the tightness of particles, and the compaction rate is mainly influenced by the particle size.

5.5 The influence of abnormally high pressure on sandstone mechanical compaction

During the burial process of clastic sediments from early deposition to mid-deep strata, abnormally high pressure is mainly formed by tectonic evolution, disequilibrium compaction, hydrothermal pressurization, clay mineral transformation, and hydrocarbon generation (Akrout et al. 2012). It inhibits compaction and protects primary pores and is of great significance to the development of mid-deep high quality reservoirs (Hunt 1990; Ma et al. 2011; Bloch et al. 2002; Cao et al. 2014).

In this paper, undercompaction simulation experiments with pressure coefficients of 1.2 and 1.4 were conducted on sample VI from the Silver Beach of Qingdao, eastern China (the same parameters as sample I) and sample VII from the Yellow River Estuary of Dongying, eastern China (the same parameters as sample IV), respectively, under an overburden pressure larger than 34 MPa. Then the experimental results were compared with those of sample I and sample IV under normal compaction, and the influence of abnormally high pressure on sandstone mechanical compaction was analyzed.

Experimental results show that the mechanical compaction rate under abnormally high pressure is obviously smaller than that under normal compaction; moreover, the higher the pressure coefficient, the greater the difference between the evolution trend line of actual porosity under

Table 8 Data about the influence of sorting on sandstone mechanical compaction

Sample no.	II	III
Average particle size *M*, mm	0.262	0.293
Sorting coefficient *So*	1.575	1.86
Primary porosity Φ_0, %	42.92	37.37
Porosity loss during rapid compaction stage, %/2.3 MPa	0.334	0.866
Porosity loss during slow compaction stage, %/2.3 MPa	0.156	0.127

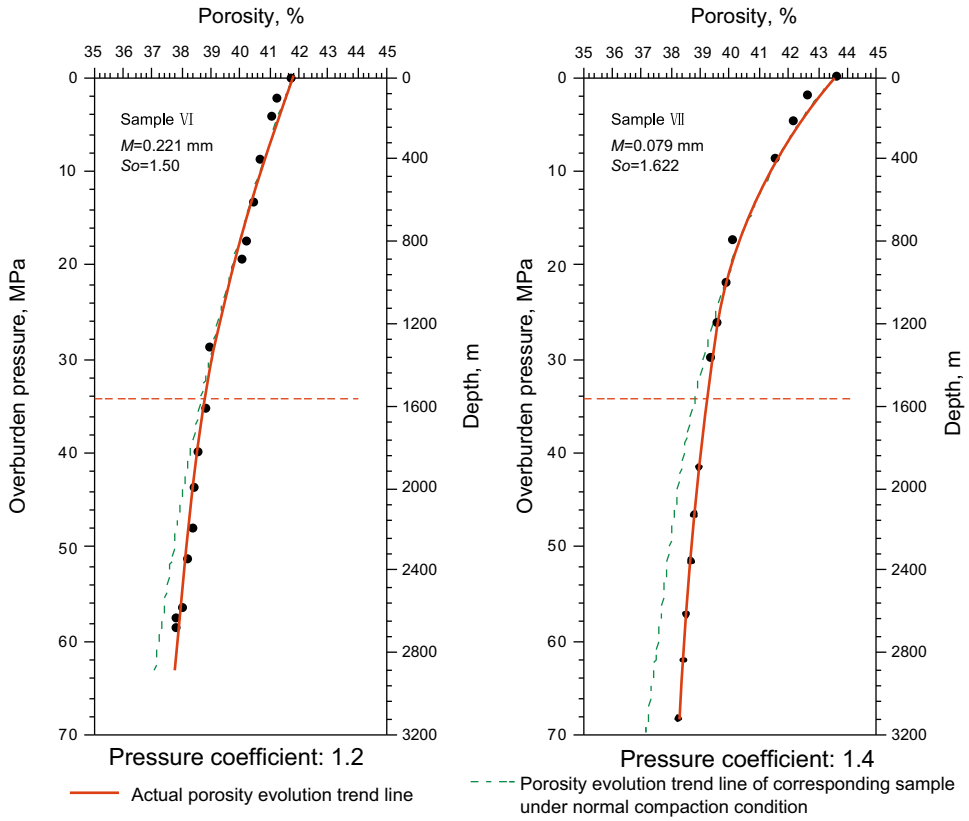

Fig. 7 Influence of formation overpressure on sandstone mechanical compaction

Table 9 Data about the influence of abnormally high pressure on sandstone mechanical compaction

Sample no.	VII	VI
Average particle size *M*, mm	0.079	0.221
Sorting coefficient *So*	1.622	1.5
Pressure coefficient	1.4	1.2
Average porosity reduction of normal compacted sample, %/2.3 MPa	0.182	0.124
Average porosity reduction of undercompacted sample, %/2.3 MPa	0.0708	0.094

abnormally high pressure and that under normal compaction (Fig. 7).

The development of abnormally high pressure is in the slow compaction stage. Experimental results show that when the pressure coefficient is 1.4, the average porosity loss of the normally compacted sample and the undercompacted sample is 0.182 % and 0.0708 %, respectively, per 2.3 MPa increase of overburden pressure. The porosity loss of the normally compacted sample is 2.571 times that of the undercompacted sample. When the pressure coefficient is 1.2, the average porosity loss of the normally compacted sample and the undercompacted sample is 0.124 % and 0.094 %, respectively, per 2.3 MPa increase of overburden pressure. The porosity loss of the normal compacted sample is 1.305 times that of the undercompacted sample (Table 9). Therefore, abnormally high pressure inhibits sandstone mechanical compaction. The higher the pressure coefficient, the slower the compaction rate. The compaction rate increases twofold when the pressure coefficient decreases by 0.2.

Further studies show that the compaction rate of sample VII with finer particle size and poorer sorting is larger than that of sample VI with coarser particle size and better sorting under normal compaction condition, which accords with particle size and sorting influencing sandstone mechanical compaction. However, when abnormally high pressure develops, the compaction rate of sample VII with a pressure coefficient of 1.4 is smaller than that of sample VI with a pressure coefficient of 1.2 in the undercompaction condition. Sandstone mechanical compaction is

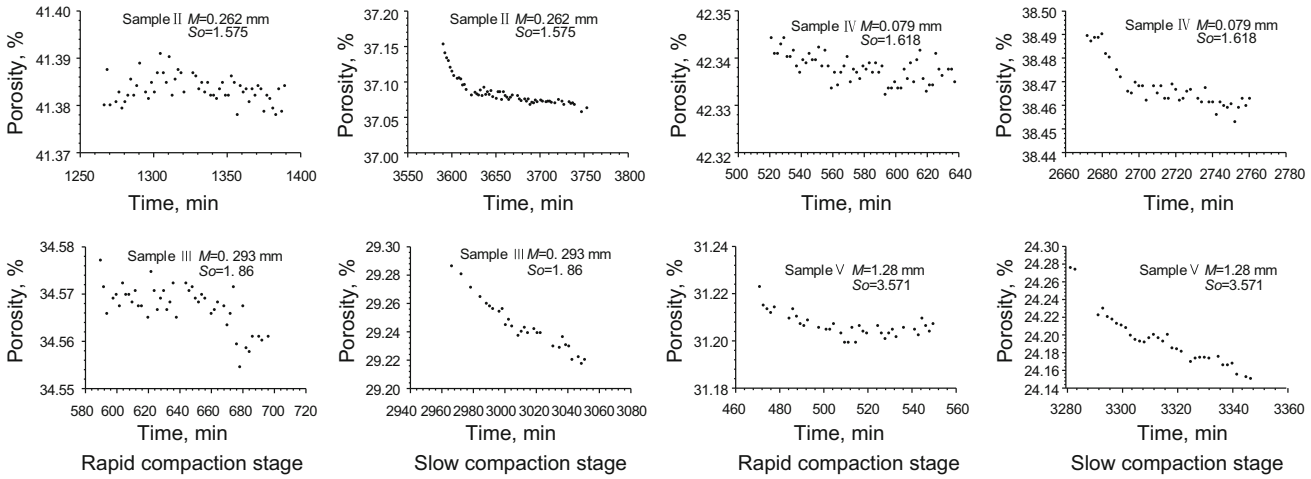

Fig. 8 Influence of burial time on sandstone mechanical compaction

Table 10 Data about the influence of burial time on sandstone mechanical compaction

Sample no.	II	III	IV	V
Average particle size *M*, mm	0.262	0.293	0.079	1.28
Sorting coefficient *So*	1.575	1.86	1.618	3.571
Porosity loss, %/h	0.389	0.349	0.229	0.119

mainly controlled by abnormally high pressure, which does not accord with particle size and sorting influencing mechanical compaction. Therefore, the control of abnormally high pressure on mechanical compaction is stronger than that of particle size and sorting.

5.6 The influence of burial time on sandstone mechanical compaction

Clastic sediments experiencing different burial time suffer different compaction effects under the same overburden pressure (Liu et al. 2007). By analyzing the experimental data at the final pressure point of rapid compaction stage and slow compaction stage during the simulation experiment, it is concluded that there is no evident correlation between porosity and compaction time during the rapid compaction stage, while a good negative relation exists between them during the slow compaction stage. Moreover, the longer the compaction time, the slower the rate of porosity reduction under the constant overburden pressure (Fig. 8). Quantitative calculations show that when the overburden pressure of the final pressure point during the slow compaction stage is constant, the porosity reduction caused by compaction per hour can be as high as 0.119 %–0.389 %, and porosity reduction caused by compaction is mainly controlled by the average particle size (Table 10). Therefore, during geological time, burial time and burial depth are the two equivalently important factors influencing sandstone mechanical compaction, and the influence of time is mainly reflected in the slow compaction stage. Only after the particles are in close contact with each other, can the creep characteristics of formation be shown with increasing compaction time.

6 Conclusions

1. There is a logarithmic relationship between primary porosity and particle size as well as sorting, and the binary function relation between primary porosity and the two factors is $\Phi_0 = -3.0413So - 3.4907\,M + 47.828123$, which can provide reference for the calculation of primary porosity of sandstone reservoir.
2. During sandstone mechanical compaction, the evolution of porosity and permeability has a segmentation characteristic with the increasing overburden pressure and depth, and the evolution curves can be divided into two sections, i.e., a rapid compaction stage with a steep slope at the earlier stage and a slow compaction stage at the later stage. The dividing pressure of two sections is about 12 MPa. During the slow compaction stage, there is an exponential relationship between porosity and overburden pressure, while a power function relationship exists between permeability and overburden pressure. The relationship between porosity and permeability is exponential.
3. The influence of particle size on mechanical compaction is mainly reflected in the slow compaction stage. The coarser the particle size, the slower the compaction rate and the larger the final porosity. The influence of particle size is more pronounced with increasing depth and overburden pressure.

4. The influence of sorting on sandstone mechanical compaction is mainly in the rapid compaction stage. The poorer the sorting, the higher the compaction rate and the more distinct the difference between the rapid compaction stage and the slow compaction stage. The dividing overburden pressure value of the two stages will be larger.
5. Abnormally high pressure inhibits sandstone mechanical compaction. The higher the pressure coefficient, the slower the compaction rate. The control of abnormally high pressure on sandstone mechanical compaction is stronger than that of particle size and sorting.
6. During geological time, burial time and burial depth are the two equivalently important factors influencing sandstone mechanical compaction. The influence of burial time is mainly reflected in the slow compaction stage, and porosity reduction caused by compaction is mainly controlled by the average particle size.
7. Although the experiments cannot be compared completely with real geological processes, they can provide some useful guidance for understanding the real geological processes. Further study should focus on simulating longer geological time by changing the pressure and temperature conditions.

Acknowledgments This study is co-funded by the National Natural Science Foundation of China (Grant No. U1262203), the National Science and Technology Special Grant (Grant No. 2011ZX05009-003), the Fundamental Research Funds for the Central Universities (Grant No. 14CX06013A), and the Chinese Scholarship Council (No. 201406450019).

References

Ajdukiewicz JM, Nicholson PH, Esch WL. Prediction of deep reservoir quality using early diagenetic process models in the Jurassic Norphlet Formation, Gulf of Mexico. AAPG Bull. 2010;94(8):1189–227.

Akrout D, Ahmadi R, Mercier E, et al. Natural hydrocarbon accumulation related to Formation overpressured interval; study case is the Saharan platform (Southern Tunisia). Arab J Geosci. 2012;5(4):849–57.

Aplin AC, Matenaar IF, McCarty DK, et al. Influence of mechanical compaction and clay mineral diagenesis on the microfabric and pore-scale properties of deep-water Gulf of Mexico mudstones. Clays Clay Miner. 2006;54(4):500–14.

Beard DC, Weyl PK. Influence of texture on porosity and permeability of unconsolidated sand. AAPG Bull. 1973;57(2):349–69.

Bloch S, Lander RH, Bonnell L. Anomalously high porosity and permeability in deeply buried sandstone reservoirs: origin and predictability. AAPG Bull. 2002;86(2):301–28.

Cao YC, Yuan GH, Li XY, et al. Characteristics and origin of abnormally high porosity zones in buried Paleogene clastic reservoirs in the Shengtuo area, Dongying Sag, East China. Petrol Sci. 2014;11(3):346–62.

Chester JS, Lenz SC, Chester FM, et al. Mechanisms of compaction of quartz sand at diagenetic conditions. Earth Planet Sci Lett. 2004;220(3–4):435–51.

Dai JX, Ni YY, Wu XQ. Tight gas in China and its significance in exploration and exploitation. Petrol Explor Dev. 2012;39(3):277–84.

Folk RL, Ward WC. Brazos River bar: a study in the significance of grain size parameters. J Sediment Petrol. 1957;27(1):3–26.

Gluyas J, Cade CA. Prediction of porosity in compacted sands. AAPG Memoir. 1999;69:19–27.

Hart BS. Seismic expression of fracture-swarm sweet sports, Upper Cretaceous tight-gas reservoirs, San Juan Basin. AAPG Bull. 2006;90(10):1519–34.

Hu ZW, Huang SJ, Wang DH, et al. Application of multiple stepwise regression to influential evaluation of pore-throat size on low-permeability sandstone reservoirs. J Guilin Univ Technol. 2013;33(1):21–5 **(in Chinese)**.

Hunt JM. Generation and migration of petroleum from abnormally pressured fluid compartments. AAPG Bull. 1990;74(1):1–12.

Jia CZ, Zheng M, Zhang YF. Unconventional hydrocarbon resources in China and the prospect of exploration and development. Petrol Explor Dev. 2012;39(2):139–46.

Liu GY, Jin ZJ, Zhang LP. Simulation study on clastic rock diagenetic compaction. Acta Sedimentol Sin. 2006;24(3):408–13 **(in Chinese)**.

Liu H, Cao YC, Jiang ZX, et al. Distribution characteristics of evaporates and Formation pressure of the fourth member of the Shahejie Formation in the Dongying Sag, the Bohai Bay Basin. Oil Gas Geol. 2009;30(3):287–93 **(in Chinese)**.

Liu MJ, Liu Z, Liu JJ, et al. Coupling relationship between sandstone reservoir densification and hydrocarbon accumulation: a case from the Yanchang Formation of the Xifeng and Ansai areas, Ordos Basin. Petrol Explor Dev. 2014;41(2):185–92.

Liu Z, Shao XJ, Jin B, et al. Co-effect of depth and burial time on the evolution of porosity for clastic rocks during the stage of compaction. Geoscience. 2007;21(1):125–32 **(in Chinese)**.

Lv ZX, Liu SB. Ultra-tight sandstone diagenesis and mechanism for the Formation of relatively high-quality reservoir of Xujiahe Group in western Sichuan. Acta Petrol Sin. 2009;25(10):2373–83 **(in Chinese)**.

Ma XM, Zhao ZY, Liu HW. Influences of abnormal overpressure on super-low permeability reservoirs in Chexi depression in Shandong. J Central South Univ (Sci Technol). 2011;42(8):2507–13 **(in Chinese)**.

Maast TM, Jahren J, Bjorlykke K. Diagenetic controls on reservoir quality in Middle to Upper Jurassic sandstones in the South Viking Graben, North Sea. AAPG Bull. 2011;95(11):1937–58.

Rogers JJ, Head WB. Relationships between porosity, median size, and sorting coefficients of synthetic sands. J Sediment Petrol. 1961;31(3):467–70.

Taylor TR, Giles MR, Hathon LA, et al. Sandstone diagenesis and reservoir quality prediction: models, myths, and reality. AAPG Bull. 2010;94(8):1093–132.

Tobin RC, McClain T, Lieber RB, et al. Reservoir quality modeling of tight-gas sands in Wamsutter field: integration of diagenesis, petroleum systems, and production data. AAPG Bull. 2010;94(8):1229–66.

Wang B, Feng Y, Zhao YQ, et al. Determination of hydrocarbon charging history by diagenetic sequence and fluid inclusions: a

case study of the Kongquehe area in the Tarim Basin. Acta Geol Sin. 2015;89(3):876–86.

Wang YJ, Tian ZY. Oil and gas exploration potential and prospect of basins in eastern area of North China. Acta Petrol Sin. 2003;24(4):7–12 **(in Chinese)**.

Wang ZM, Liu LF, Yang HJ, et al. Characteristics of Paleozoic clastic reservoirs and the relationship with hydrocarbon accumulation in the Tazhong area of the Tarim Basin, west China. Petrol Sci. 2010;7(2):192–200.

Worden RH, Mayall M, Evans IJ. The effect of ductile-lithic sand grains and quartz cement on porosity and permeability in Oligocene and lower Miocene clastics, South China Sea: prediction of reservoir quality. AAPG Bull. 2000;84(3):345–59.

Yuan EX. Engineering fluid mechanics. Beijing: Petroleum Industry Press; 1985. p. 8 **(in Chinese)**.

Zhang N, Tian ZJ, Wu SH, et al. Study Xujiahe reservoir diagenetic process, Sichuan Basin. Acta Petrolog Sin. 2008;24(9):2179–84 **(in Chinese)**.

Zhang Q, Zhu XM, Ronald JS, et al. Variation and mechanisms of clastic reservoir quality in the paleogene shahejie Formation of the Dongying Sag, Bohai Bay Basin, China. Petrol Sci. 2014;11(2):200–210.

Zhang SC, Zhang BM, Li BL, et al. History of hydrocarbon accumulations spanning important tectonic phases in marine sedimentary basins of China: taking the Tarim Basin as an example. Petrol Explor Dev. 2011;38(1):1–15.

Zhu HH, Zhong DK, Li QR, et al. Characteristics and controlling factors of upper Triassic Xujiahe tight sandstone reservoir in southern Sichuan Basin. Acta Sedimentol Sin. 2013;31(1):167–75 **(in Chinese)**.

Zhu RK, Zou CN, Zhang N, et al. Diagenetic fluids evolution and genetic mechanism of tight sandstone gas reservoirs in Upper Triassic Xujiahe Formation in Sichuan Basin, China. Sci China Ser D. 2008;51(9):1340–53.

Zou CN, Zhang GS, Yang Z, et al. Geological concepts, characteristics, resource potential and key techniques of unconventional hydrocarbon: on unconventional petroleum geology. Petrol Explor Dev. 2013;40(4):385–99 **(in Chinese)**.